Separation Techniques

DOI: 10.1002/anie.200805396

Compartmentalization of Chemically Separated Components into Droplets **

*J. Scott Edgar, Graham Milne, Yiqiong Zhao, Chaitanya P. Pabbati, David S. W. Lim, and Daniel T. Chiu**

Microscale chemical separation plays a prominent role in biotechnology and chemical analysis. In microscale separation, much effort is spent to separate individual analyte species of a complex mixture into distinct bands. After the detection of each band, however, the separated components often cannot be easily preserved for additional analysis or manipulation owing to molecular diffusion. This challenge is especially acute in high-resolution separation techniques, such as capillary electrophoresis (CE) and microscale high-performance liquid chromatography (micro-HPLC), because of the extremely small volumes and narrow bands involved. Herein, we describe a new concept based on the use of droplets to compartmentalize the separated bands, thus preventing the dilution and loss of the separated components and facilitating their downstream manipulation and analysis.

In high-resolution microscale separation, such as CE, sample volumes are often in the nanoliter[1,2] or even femtoliter range,[3–5] so that the number of theoretical plates is often in the millions.[6] In such systems, it has been extremely difficult to maintain the contents of the separated peaks after their detection. Experimental advances, however, have been made to address this issue.[6–9] Zare and co-workers, for example, employed elastomeric valving and subnanoliter chambers to capture separated bands for single-molecule studies,[7,8] whereas Zaleweski et al. used electrokinetic flow switching to collect separated CE fractions.[9] By integrating droplet generation induced by electroosmotic flow (EOF) with chemical separation, we have used droplets to spatially confine components separated by CE. Although we have focused on CE separation, we believe this concept can be applied broadly to other high-resolution techniques in microscale chemical separation.

Droplets have emerged in the past few years as a platform for a wide range of applications, some of which are based on the use of monodisperse droplets generated by using microfluidics,[10–13] others on the use emulsion systems.[14,15] A schematic illustration of the concept of spatially confining separated bands into droplets is shown in Figure 1a. Figure 1b shows the particular fluidic design that we used to compartmentalize CE-separated bands (see the Supporting Information for experimental details). The chip used consisted of three regions: a sample-injection region, a CE-separation channel, and a droplet-formation region. The cross-section of the sample-injection channel was 3×3 μm, and the cross-section of the CE channel was 10×10 μm. The droplet-formation region comprised two oil channels (50×50 μm) that flanked the CE channel, and an exit channel that was 50 μm high and 100 μm wide (Figure 1c). EOF in the CE channel was initiated by applying a high voltage to the platinum electrode and by grounding the indium tin oxide (ITO) electrode on the floor of the microchannel. In the absence of an applied voltage, the aqueous/oil interface was balanced, and no droplet formation occurred.

To characterize the effect of droplet formation on CE separation, we monitored the separated bands at three locations during three separate injections (Figure 1b). The electropherogram recorded at the first detection spot before the ITO electrode shows that all amino acids were separated by CE except for D- and L-glutamate (Figure 1d). To further resolve the D/L-glutamate peak, we transferred the contents of the droplets containing D/L-glutamate into a fused silica capillary for a second-dimension separation by micellar electrokinetic chromatography (MEKC). The inset in Figure 1d shows the D- and L-glutamate peaks after this second-dimension MEKC separation. The L-glutamate peak is more intense than the D-glutamate peak because we intentionally introduced more dye-tagged L-glutamate into the sample to enable us to identify the two peaks on the basis of their relative intensities.

Figure 1e shows the electropherogram recorded at the second detection spot after the ITO electrode. Upon enlargement of one of the peaks (inset), a series of small peaks or oscillations were seen to be superimposed on the main peak. The frequency of oscillation was identical to the frequency of droplet generation. We discuss the origin of this oscillation in the next section. Figure 1f shows the peaks detected at the third detection spot, located after the droplet-generation region. Expansion of the D/L-glutamate peak (inset) revealed the presence of many individual peaks; each of these peaks corresponds to a droplet.

Our device employed a modified flow-focusing design, in which droplet generation was driven by EOF (Figure 1b,c). For our EOF-induced droplet generation, we can estimate the maximum absolute pressure (ΔP_{max}) generated by EOF in our CE channel:[16] $\Delta P_{max} = 32\,\varepsilon_0\varepsilon_r\zeta U w^{-2}$. In this equation, ε_0 is the electrical permittivity of a vacuum, ε_r is the relative permittivity of the medium, ζ is the zeta potential of the

[*] J. S. Edgar, Dr. G. Milne, Dr. Y. Zhao, C. P. Pabbati, Dr. D. S. W. Lim, Prof. D. T. Chiu
Department of Chemistry, University of Washington
Box 351700, Seattle, WA 98195-1700 (USA)
Fax: (+1) 206-685-8665
E-mail: chiu@chem.washington.edu

[**] We gratefully acknowledge support of this research by the National Institutes of Health (EB005197).

Supporting information for this article is available on the WWW under http://dx.doi.org/10.1002/anie.200805396.

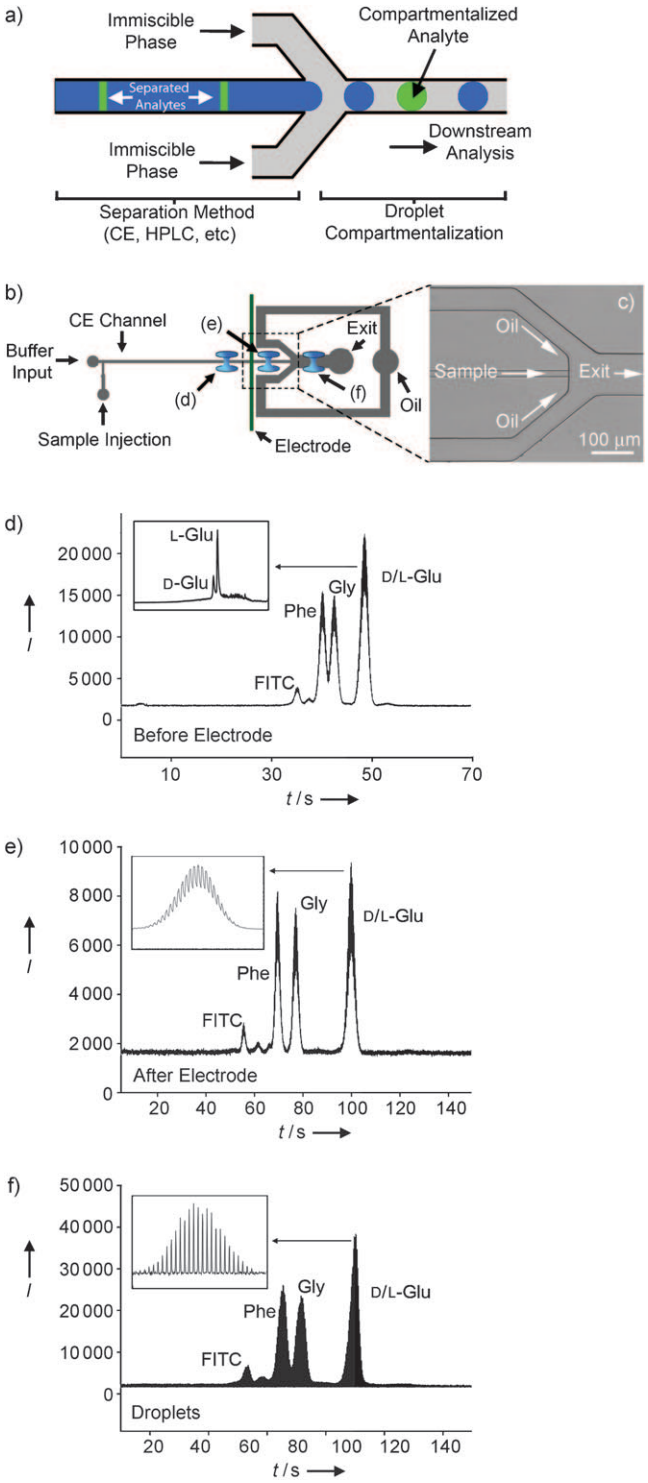

Figure 1. Droplet compartmentalization of the components of a mixture separated by capillary electrophoresis (CE). a) Schematic representation of the general method used for the compartmentalization of the separated bands in droplets. b) Schematic representation of the fluidic design used to integrate CE with droplet compartmentalization. The locations of the confocal detection spots are depicted as three blue laser foci. c) Droplet-formation region shown in detail. Oil channels: 50×50 μm; exit channel: 50×100 μm; CE channel (sample): 10×10 μm. d) Electropherogram recorded before the indium tin oxide (ITO) electrode (separation buffer: 20 mM borate at pH 9; applied field: 350 Vcm^{-1}). As the D- and L-glutamate could not be separated in free solution, droplets that compartmentalized the D/L-glutamate peak were removed from the chip at the exit reservoir and then injected into a fused silica capillary (10 μm internal diameter) for separation by micellar electrokinetic chromatography (separation buffer: 20 mM borate, 30 mM sodium dodecyl sulfate, 20 mM β-cyclodextran; applied field: 250 Vcm^{-1}). e) Electropherogram recorded after the ITO electrode. f) Electropherogram recorded after droplet generation. FITC: fluorescein isothiocyanate; Phe: FITC–phenylalanine; Gly: FITC–glycine; D/L-Glu: FITC-labeled D- and L-glutamate. The immiscible phase was AR20 silicone oil.

poly(dimethylsiloxane) (PDMS) channel wall, U is the applied voltage, and w is the width of the channel. By using literature values of 8.85×10^{-12} $C^2N^{-1}m^{-2}$ for ε_0, 80 for ε_r, and −50 mV for ζ, and the values of U (1 kV) and w (10 μm) from our experiments, we estimate a ΔP_{max} value of approximately 11 kPa.[16] This value is consistent with the hydrodynamic pressure needed to produce droplets in the frequency range of kHz in a standard flow-focusing device.[17]

To understand the observed frequency oscillations, we imaged the droplet-formation process by using a fast camera (Figure 2a–d). From this series of images, it is evident that the aqueous/oil interface always advanced in the CE channel during droplet formation and never retracted beyond its initial position at the start of the droplet-formation cycle (Figure 2a,d). We also noticed that the flow rate of the aqueous phase was inhomogeneous. Whereas the flow rate was fast during droplet formation (Figure 2b), it was slow during the initial advance of the interface within the CE channel (Figure 2a) and also during necking of the droplet (Figure 2c). From Figure 2a–d, we estimate that the average EOF mobility in our CE channel was approximately 5.9×10^{-4} $cm^2V^{-1}s^{-1}$, which is similar to values found previously for oxidized PDMS channels.[4] We estimated the average EOF mobility when the interface was confined within the CE channel (we term this state the bounded interface) to be approximately 2.7×10^{-4} cm^2 $V^{-1}s^{-1}$ and thus almost three times slower than when the interface entered the large exit oil channel (unbounded interface) during droplet formation (EOF $\approx 7.3\times10^{-4}$ $cm^2V^{-1}s^{-1}$). We therefore hypothesized that this slow–fast motion of the aqueous phase in the CE channel was responsible for the oscillations: When the flow was slow, there was more photobleaching of the dye in the laser probe volume, which led to a lower detected fluorescence, but when the flow was fast, photobleaching was minimized, which resulted in a larger detected signal.

To test this hypothesis, we detected the fluorescence signal from the CE channel and imaged the droplet-formation process simultaneously (Figure 2e). For this purpose, the laser spot for fluorescence detection was placed just upstream of droplet formation. (The bright spot in inset III is the laser focus.) In this experiment, the entire CE channel was filled with fluorescein. Under uniform EOF, we observed a constant fluorescence signal. With a variable flow rate and photobleaching, however, the detected fluorescence changed. Figure 2e correlates this change in the detected fluorescence signal with the different stages of droplet formation. When the interface was bounded in the CE channel (inset I), the

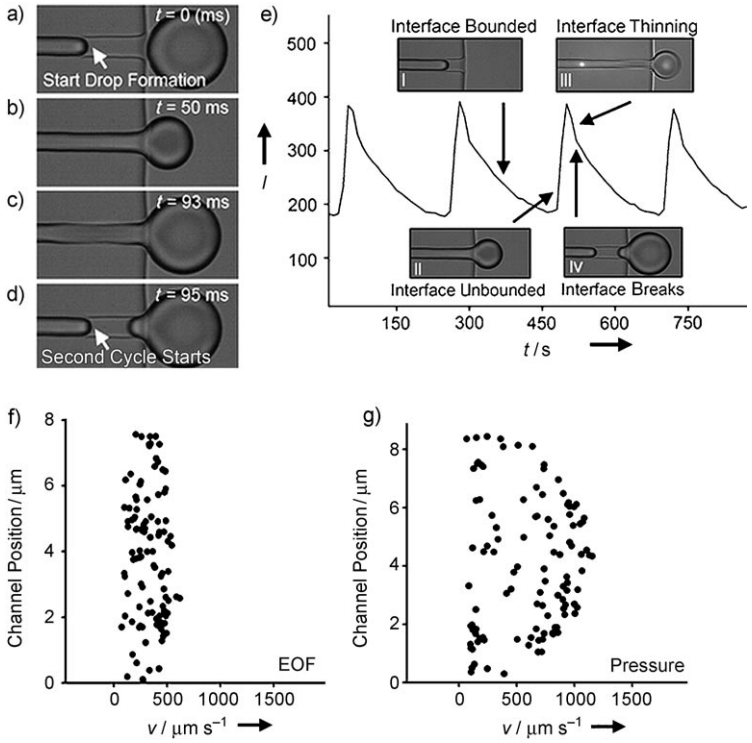

Figure 2. Dynamics of droplet generation induced by electroosmotic flow (EOF). a–d) Sequence of images showing EOF-induced droplet formation (applied field: 350 Vcm^{-1}). e) Simultaneous confocal detection (the bright spot in inset III marks the location of the laser focus) of fluorescence from the separation channel and imaging of droplet formation. In this case, the entire separation channel was filled with fluorescein at a homogeneous concentration (1 µM fluorescein in 20 mM borate, pH 9). f, g) Mapping of the flow profile during droplet formation by particle velocimetry. The flow profiles in (f) and (g) were averaged over 10 cycles of droplet formation. The immiscible oil phase was AR20 silicone oil for all experiments.

flow rate was slow, and thus the detected signal was low as a result of photobleaching. The detected fluorescence increased rapidly as the interface became unbounded and as the droplet grew in size (inset II). During necking (inset III) and droplet break-off (inset IV), as marked by the inflection point in the detected signal, flow again slowed, which resulted in a decrease in the recorded fluorescence. This cycle repeats itself with the formation of each droplet; Figure 2e shows the signal trace from four cycles of droplet generation.

The change in flow velocity between the two regimes (bounded versus unbounded interface) was caused by a decrease in pressure at the interface as the droplet was formed, as governed by the Young–Laplace equation:[18] $\Delta P_{lap} = 4\gamma/d$. In this equation, ΔP_{lap} is the Laplace pressure, γ is the interfacial tension, and d is the diameter of the droplet. As a droplet forms, the increase in diameter causes a continual decrease in pressure at the interface.[18] This decrease in pressure leads to an increase in flow rate, which eventually results in necking and finally droplet break-off.

Because the growing droplet is entrained by the flowing immiscible oil phase, we were concerned that the plug-flow profile of EOF would be perturbed within the CE channel. Therefore, we used particle velocimetry to map the flow profile in the CE channel during EOF-driven droplet formation. Our results clearly indicated that the plug flow in the CE channel was unaffected by droplet generation (Figure 2f). As a control, we also applied hydrodynamic pressure to the CE channel. A parabolic flow profile resulted as anticipated (Figure 2g). Therefore, we conclude that droplet formation does not affect the plug-flow profile of CE. Although the EOF velocity is not homogeneous during droplet formation, the electrophoresis component of CE is homogeneous and constant. As a result, the separation efficiency of CE is not affected by downstream droplet generation.

The frequency and size of the droplets formed depended both on the strength of the applied electric field and the flow rate of the continuous immiscible phase (Figure 3a,b). At a given continuous-phase flow rate, higher voltages led to an increase in the EOF rate and thus an increase in both the rate at which the droplets were generated and the volume of the droplets. For a given applied field strength and thus EOF rate, an increase in the continuous-phase flow rate led to an increase in the frequency of droplet generation but to a decrease in the volume of the droplet formed. This behavior is expected, because at a given EOF rate, the volume of each droplet must decrease to support the higher frequency of droplet formation. We also noticed that droplet formation could be tuned over a wide range by using different immiscible fluids. For example, under identical operating conditions, the frequency at which droplets were formed and the volume of the droplets were 10 Hz and 0.3 nL in

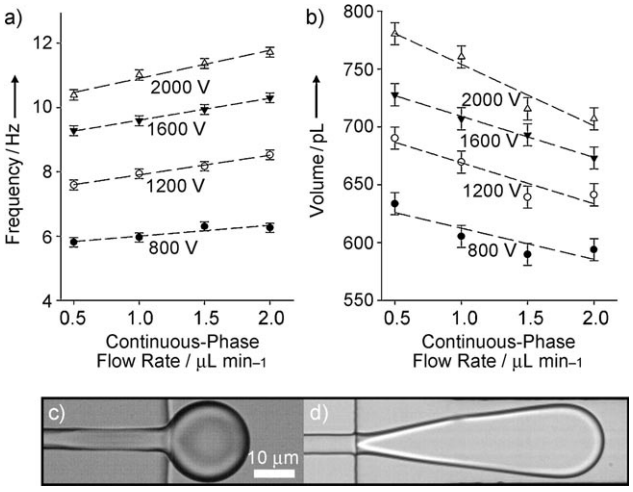

Figure 3. Tuning of the frequency of droplet formation and droplet size. a,b) Plots showing the dependence of a) the frequency of droplet generation and b) droplet volume on the applied field strength and the flow rate of the immiscible oil phase. The aqueous phase was 20 mM borate buffer (pH 9), and the immiscible phase was AR20. c, d) EOF-induced droplet formation in c) AR20 silicone oil and d) fluorinert FC40. In both (c) and (d), the aqueous phase was 20 mM borate buffer (pH 9), the applied field strength was approximately 350 Vcm^{-1}, and the oil flow rate was 1.0 µL min^{-1}.

AR20 silicone oil (Figure 3c) but changed to 0.3 Hz and 1 nL when fluorinert FC40 was used (Figure 3d). Therefore, the frequency of droplet formation and the size of the droplets can be adjusted so that a separated peak is confined in one droplet or in many droplets.

Depending on the particular application, the droplet-confined peaks might need to be analyzed further on the chip or removed from the chip for additional separation (Figure 1d) or assay. For further on-chip analysis, the droplets would need to be docked and stored in a spatially defined manner after chemical separation. Figure 4a shows one possible scheme, in which the droplets were trapped sequentially in a series of docking sites along a serpentine channel after CE. Figure 4b outlines the operation of the serpentine droplet-docking channel.[19,20] The order in which the droplets leave the CE channel is encoded in their docking positions, whereby the first droplet to leave the CE channel is docked first. Figure 4c shows a series of droplets docked in this manner. To illustrate the use of droplet docking for trapping a desired band in the CE channel, we used a cylindrically focused UV laser pulse (3 ns at 355 nm) to uncage a sharp band ($\approx$2 μm wide) of caged fluorescein in a procedure similar to established procedures used in optically gated injection.[21] This band was then transported down the CE channel by EOF, encapsulated in a droplet, and then docked in the serpentine channel (Figure 4d–f).

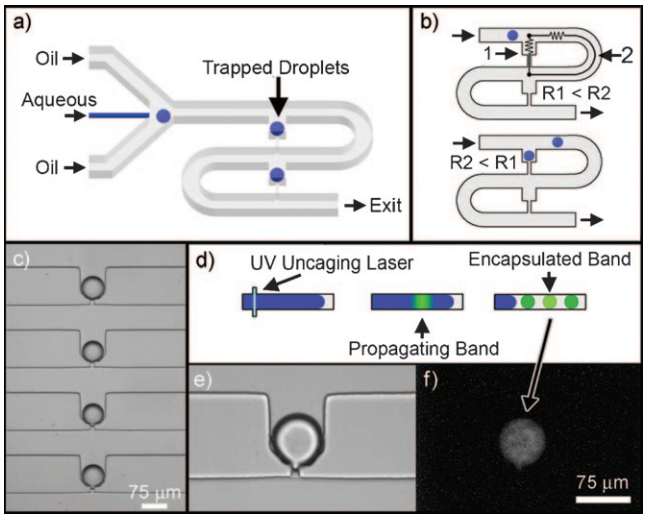

Figure 4. Droplet docking. a) Schematic representation of the chip design used to integrate separation by capillary electrophoresis (CE) with droplet compartmentalization and docking. b) Fluidic circuit diagram for droplet docking. The small constriction that prevented the docked droplet from passing through was 15 μm long × 10 μm wide × 10 μm high, whereas the rest of the channel was 75 μm wide × 50 μm high. c) Docked droplets generated by electroosmotic flow at the junction of the CE and oil channels. d) Schematic representation of the UV uncaging of caged fluorescein in the CE channel to create a narrow band of fluorescein. e) Bright-field and f) fluorescence images that show that the uncaged band of fluorescein was captured in a droplet and docked in the array.

High-resolution and high-sensitivity techniques in micro-scale chemical separation, such as CE and micro-HPLC, are playing an increasingly important role in biotechnology and cellular analysis. The concept presented herein offers an approach to overcome molecular diffusion by confining the separated bands in a series of droplets, which can be further manipulated and studied on chip or removed from the chip for analysis. We anticipate that this approach will open new possibilities for the analysis of complex cellular components separated by CE and other high-resolution chromatographic techniques.

Received: November 5, 2008
Published online: January 13, 2009

Keywords: analytical methods · capillary electrophoresis · droplets · electroosmotic flow · microfluidics

[1] D. L. Olson, T. L. Peck, A. G. Webb, R. L. Magin, J. V. Sweedler, *Science* **1995**, *270*, 1967.
[2] C. A. Monnig, R. T. Kennedy, *Anal. Chem.* **1994**, *66*, 280.
[3] P. G. Schiro, C. L. Kuyper, D. T. Chiu, *Electrophoresis* **2007**, *28*, 2430.
[4] J. S. Edgar, C. P. Pabbati, R. M. Lorenz, M. Y. He, G. S. Fiorini, D. T. Chiu, *Anal. Chem.* **2006**, *78*, 6948.
[5] G. T. Roman, M. Wang, K. N. Shultz, C. Jennings, R. T. Kennedy, *Anal. Chem.* **2008**, *80*, 8231.
[6] J. Kraly, M. A. Fazal, R. M. Schoenherr, R. Bonn, M. M. Harwood, E. Turner, M. Jones, N. J. Dovichi, *Anal. Chem.* **2006**, *78*, 4097.
[7] S. Kim, B. Huang, R. N. Zare, *Lab Chip* **2007**, *7*, 1663.
[8] B. Huang, H. K. Wu, D. Bhaya, A. Grossman, S. Granier, B. K. Kobilka, R. N. Zare, *Science* **2007**, *315*, 81.
[9] D. R. Zalewski, S. Schlautmann, R. B. M. Schasfoort, H. Gardeniers, *Lab Chip* **2008**, *8*, 801.
[10] H. Song, D. L. Chen, R. F. Ismagilov, *Angew. Chem.* **2006**, *118*, 7494; *Angew. Chem. Int. Ed.* **2006**, *45*, 7336.
[11] A. Huebner, S. Sharma, M. Srisa-Art, F. Hollfelder, J. B. Edel, A. J. Demello, *Lab Chip* **2008**, *8*, 1244.
[12] M. J. Fuerstman, P. Garstecki, G. M. Whitesides, *Science* **2007**, *315*, 828.
[13] A. S. Utada, E. Lorenceau, D. R. Link, P. D. Kaplan, H. A. Stone, D. A. Weitz, *Science* **2005**, *308*, 537.
[14] J. S. Kuo, P. Spicar-Mihalic, I. Rodriguez, D. T. Chiu, *Langmuir* **2003**, *19*, 250.
[15] M. Margulies et al., *Nature* **2005**, *437*, 376.
[16] I. M. Lazar, B. L. Karger, *Anal. Chem.* **2002**, *74*, 6259.
[17] T. Ward, M. Faivre, M. Abkarian, H. A. Stone, *Electrophoresis* **2005**, *26*, 3716.
[18] I. Kobayashi, S. Mukataka, M. Nakajima, *Langmuir* **2004**, *20*, 9868.
[19] W. H. Tan, S. Takeuchi, *Proc. Natl. Acad. Sci. USA* **2007**, *104*, 1146.
[20] W. Shi, J. Qin, N. Ye, B. Lin, *Lab Chip* **2008**, *8*, 1432.
[21] P. H. Paul, M. G. Garguilo, D. J. Rakestraw, *Anal. Chem.* **1998**, *70*, 2459.

